



**HAL**  
open science

# Novel Polyimide-Based Conformal Bandpass FSS for X-band RADAR Communications

Geethanjali Govindarajan, Preetha Purusothaman

► **To cite this version:**

Geethanjali Govindarajan, Preetha Purusothaman. Novel Polyimide-Based Conformal Bandpass FSS for X-band RADAR Communications. JOURNAL OF HIGH-FREQUENCY COMMUNICATION TECHNOLOGIES, 2024, 2 (01), pp.130-139. 10.58399/BAAG2904 . hal-04509350

**HAL Id: hal-04509350**

**<https://hal.science/hal-04509350>**

Submitted on 18 Mar 2024

**HAL** is a multi-disciplinary open access archive for the deposit and dissemination of scientific research documents, whether they are published or not. The documents may come from teaching and research institutions in France or abroad, or from public or private research centers.

L'archive ouverte pluridisciplinaire **HAL**, est destinée au dépôt et à la diffusion de documents scientifiques de niveau recherche, publiés ou non, émanant des établissements d'enseignement et de recherche français ou étrangers, des laboratoires publics ou privés.



# Novel Polyimide-Based Conformal Bandpass FSS for X-band RADAR Communications

Geethanjali Govindarajan<sup>1\*</sup>, Preetha Purusothaman<sup>2</sup>

<sup>1,2</sup> Department of Electronics and Communication Engineering, Anna University, Chennai, India  
E-mail address: [geethanjali5699@gmail.com](mailto:geethanjali5699@gmail.com)/[23244991389@student.annauniv.edu](mailto:23244991389@student.annauniv.edu) & [preethamathi26@gmail.com](mailto:preethamathi26@gmail.com)/[24249191101@student.annauniv.edu](mailto:24249191101@student.annauniv.edu)

## Abstract

A linearly polarized wide bandpass frequency selective surface (FSS) for RADAR communication application has been presented. The proposed FSS is constructed in a single layer with a size of  $0.25 \lambda_0$ . This FSS utilizes a rhombus slot comprises a head slot and a meander line to provide a single-wideband resonance. The proposed FSS operates in the X-band communication frequency range from 7.98 to 12.1 GHz (4.12 GHz) and achieves a minimum insertion loss of 0.1 dB, respectively. The designed FSS is developed on a flexible polyimide substrate with a thickness of 0.05 mm ( $\epsilon_r = 3.5$ ,  $\tan \delta = 0.00027$ ). The FSS exhibits stable angular performance in the scope of incidence angle of  $60^\circ$  for both TE and TM modes. An equivalent circuit model is designed to depict the desired frequency response. Furthermore, a bending analysis has been carried out to verify the conformal nature of the proposed unit cell. The prototype is fabricated and the performances are validated with experimental results.

**Keywords:** Bandpass, Flexible design, frequency selective surface (FSS), X band, Bandwidth

## 1. Introduction

Owing to their excellent handling of electromagnetic (EM) waves, the FSS has garnered extensive attention in RADAR-based applications. The FSSs have been employed in the microwave field to construct spatial filters, Electromagnetic Interference (EMI) reduction, and radome [Munk and Munk; \(2000\)](#) due to their specific filtering property. The bandpass FSS can be used in the radome design for the reduction of Radar Cross Section (RCS), and due to its conformal property, it is also exploited in the military aircraft nozzle for communicating the allied forces in a specific frequency range which is the primary interest in this work. Thus, the bandpass FSS with wider bandwidth, low profile, and minimum insertion loss is required to obtain such characteristics. Several approaches have been reported to achieve these features [Cahill et al. \(2001\)](#), [Vegesna et al. \(2012\)](#), [Zhou et al. \(2016\)](#), [Sarabandi and Behdad \(2007\)](#), [Al-Joumayly and Behdad \(2009\)](#), [Wang et al. \(2016\)](#), [Chen et al. \(2021\)](#), [Li et al. \(2020\)](#), [Al-Joumayly and Behdad \(2010\)](#), [Wang et al. \(2022\)](#), [Liu et al. \(2017\)](#), [Liu et al. \(2020\)](#), [Dong et al. \(2021\)](#), [Zhou et al. \(2022\)](#), [Zhu et al. \(2018\)](#) and [Zhao et al. \(2019\)](#). A cascaded number of 2-D FSS with quarter wavelength dielectric spacers are proposed in [Cahill et al. \(2001\)](#) & [Vegesna et al. \(2012\)](#). The reported FSS is practically undesirable especially in low frequencies due to the cascaded periodic structures or high profile. The design of a substrate-integrated waveguide (SIW)-based FSS is presented in [Zhou et al. \(2016\)](#) to

\*Corresponding author

Received: 26<sup>th</sup>, January 2024, Revised: 04<sup>th</sup> March, 2024, Accepted: 09<sup>th</sup> March 2024 and available online 18<sup>th</sup> March 2024



**Table 1.** Comparison With Other Works Regarding Center Frequency Deviation with Incident Angles

References	$f_0$ (GHz)	Incident Angle	TE	TM
Li et al. (2020)	10.2	40°	7%	10 %
Abadi and Behdad (2015)	21	40°	2.8%	2.28 %
Yan et al. (2015)	10	60°	18.2%	16%
Hussein et al. (2017)	3.8	40°	2.6%	2.6%
<b>This Work</b>	10	60°	1% $T_p$	1% $T_p$

achieve a quasi-elliptic filtering response by introducing the cross-couplings. A multilayer FSS with lower insertion loss, and non-resonant subwavelength periodic structures are reported in Sarabandi and Behdad (2007) & Al-Joumayly and Behdad (2009). Advantages such as low profile, and wider transmission, are studied in this article. However, the FSS with relatively small dimensions is less sensitive to the incidence angle. Thus, the radome for miniaturized low-frequency antennas and antenna arrays are not suitable for this category. The stable angular performance is obtained by a multiple-layer planar design with cross-coupling Wang et al. (2016). The design method for obtaining the wider bandwidth using the stacked structures is investigated in Chen et al. (2021) & Li et al. (2020). The stacked unit cell employs miniaturization and stable oblique incidences. However, due to their high profile and large unit cells, they are not preferred for many applications Al-Joumayly and Behdad (2010). The 3-D bandpass FSS is reported in Wang et al. (2022) to avoid the multiple layers and bulky profile. Although this exhibits fair performances its structure is usually more complicated for the fabrication process. High selectivity with wide transmission behaviors is obtained by using multiple layers Li et al. (2020). The bandpass FSS design with feasible bandwidth compensation and wideband rejection for radome applications in dual and multiple layers is presented in Liu et al. (2017) & Liu et al. (2020). Based on the equivalent circuit model a miniaturized quad-stopband FSS is proposed in Dong et al. (2021). A narrow passband is obtained in Zhou et al. (2022) with high selectivity and angular stability. An FSS with a quasi-elliptical frequency bandpass filtering response is presented in Zhu et al. (2018) & Zhao et al. (2019). A miniaturized bandpass FSS with high-order and quasi elliptical bandpass FSS is proposed in Abadi and Behdad (2015), Yan et al. (2015), Hussein et al. (2017), Jiang et al. (2024) and Afzal et al. (2023). High profile, multiple layers, cascaded and stacked structures, or dense via arrays are required to achieve the ideal characteristics of the bandpass FSS.

Thus, to overcome the effects of the aforementioned methods a wider bandpass FSS with a low profile, minimum insertion loss, and Polarization-insensitive is presented without exploiting the needed advances from the literature Cahill et al. (2001), Vegesna et al. (2012), Zhou et al. (2016), Sarabandi and Behdad (2007), Al-Joumayly and Behdad (2009), Wang et al. (2016), Chen et al. (2021), Li et al. (2020), Al-Joumayly and Behdad (2010), Wang et al. (2022), Liu et al. (2017), Liu et al. (2020), Dong et al. (2021), Zhou et al. (2022), Zhu et al. (2018) and Zhao et al. (2019). The proposed FSS is capable of achieving a stable angular performance up to 60° for TE and TM mode polarizations. When compared with similar state-of-the-art works, the designed FSS has a wider bandwidth, low insertion loss, and better angular stability. Based on the characteristics achieved, the proposed bandpass FSS is considered a good candidate for RADAR communication application. The prototype of the bandpass FSS is fabricated and tested using a lab-made experimental setup using the pyramidal absorbers. This manuscript is organized as follows: Section 2 presents the unit cell design and characterization. Section 3 presents the performance of the conformal bandpass FSS. The fabrication and measurement of the FSS are detailed in section 4.

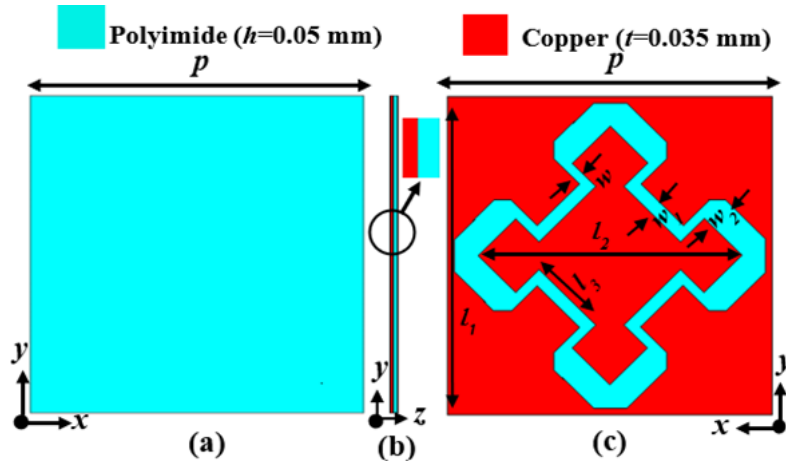


**Figure 1.** Geometry of the unit cell, (a) Front view (substrate), (b) Side view, and (c) Rear view (resistive sheet).  $P = 9.7\text{mm}$ ,  $w = 0.4\text{mm}$ ,  $l_1 = 9.3\text{mm}$ ,  $l_2 = 5.2\text{mm}$ ,  $w_1 = 0.25\text{mm}$ , and  $w_2 = 0.7\text{mm}$ ,  $l_3 = 1.5\text{mm}$

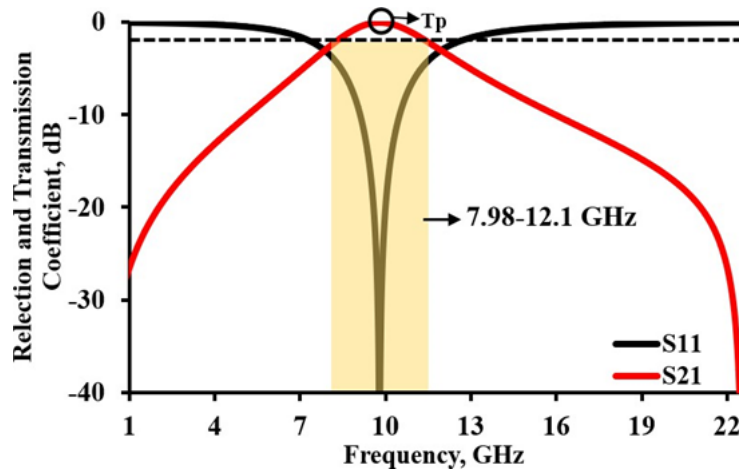


**Figure 2.** Frequency response of the simulated bandpass FSS

## 2. Design and Analysis of Conformal Bandpass FSS

### 2.1. Conformal Bandpass FSS design

The bandpass FSS is developed on a flexible polyimide substrate having a dielectric constant of 3.5 and a loss tangent of 0.027. The overall size of the unit cell is  $9.7 \times 9.7 \times 0.05$  mm. The proposed unit cell achieves wideband resonance by a single resonant structure as described in Fig. 1. The front and side views of the bandpass FSS are depicted in Fig. 1(a) and Fig. 1(b), respectively. The FSS characteristics are achieved by designing the unit cell in a single layer with a low profile. The wider transmission with lower insertion loss is produced by introducing a rhombus slot incorporated with a meander line in the resistive sheet as shown in Fig. 1(c). The desired impedance matching is achieved without exploiting the methods reported in Cahill et al. (2001), Vegesna et al. (2012), Zhou et al. (2016), Sarabandi and Behdad (2007), Al-Joumayly and Behdad (2009), Wang et al. (2016), Chen et al. (2021), Li et al. (2020), Al-Joumayly and Behdad (2010), Wang et al. (2022) and Liu et al. (2017). The resonant frequency of the design can be tuned by adjusting the width ( $w$ ) and the length ( $l_1$ ) with the optimized parameters shown in Fig. 1(b). The simulated S-parameter of the bandpass FSS is shown in Fig. 2. The transmission pole ( $T_p$ ) at 10 GHz is obtained covering the X-band ranging from 7.9 to 12.1 GHz. The maximum insertion loss (IL) through the passband is less than 0.1 dB, whereas its 3 dB bandwidth reaches 40%. The unit cell is designed using CST microwave studio. The characteristics of the transmission are

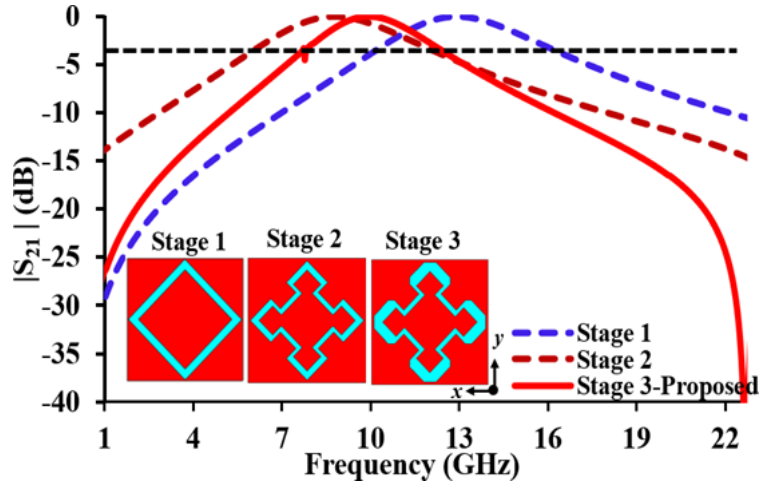


**Figure 3.** Evolution of the bandpass FSS characteristics

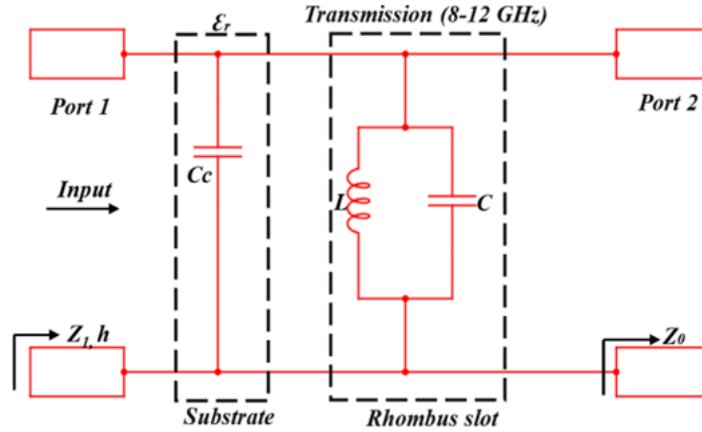


**Figure 4.** ECM of the proposed bandpass FSS. The approximate values are  $C_c$  (dielectric) = 0.508 pF,  $L = 1.08nH$ ,  $C = 2.42pF$ , and  $h = 0.05mm$

investigated using floquet mode theory. The EM wave is defined along the  $z$ -direction, while the periodic boundary conditions are defined along the  $x$  and  $y$  directions. The transmission properties are studied using uniform plane wave excitation. The  $x$  and  $y$  direction represents the unit cell and  $Z_{min}$  and  $Z_{max}$  are set to open free space. The evolution of the proposed unit cell is described in Fig. 3 and the corresponding transmission characteristics are plotted in Fig. 4. The structure of the unit cell has evolved from a rhombus slot as shown in Stage 1. Here, the length and width of the rhombus slot are determined by using half wavelength. The fundamental unit cell operates from 12 to 16 GHz with high roll-off and an insertion loss of 1.5 dB. Therefore, the rhombus slot is modified with a meander line to reduce the roll-off characteristics in high frequencies Munk and Munk; (2000) without making the unit cell large. Thus, the unit cell in Stage 2 operates from 9 to 12 GHz and achieves a minimum insertion loss of 1 dB. However, the desired RADAR frequency is not achieved. To obtain the RADAR communication frequency range, the width of the head slot increases to 0.7 mm and achieves the desired impedance matching Wang et al. (2016) with the minimum insertion loss of 0.05 dB as shown in Stage 3.

## 2.2. Equivalent circuit model

The equivalent circuit model (ECM) of the proposed bandpass FSS is depicted in Fig. 4. Based on the method reported in Liu et al. (2017) the ECM is developed. As indicated in Fig. 5 the ECM is composed of a single  $LC$  resonator. The resonant frequency (7.98-12.1 GHz) is composed of a basic parallel  $LC$  resonator ( $L - C$ ). In addition,  $Z_0$  and  $Z_1$  are the wave impedance of the

free space and the dielectric substrate, respectively. For the resonant frequency, the transmission pole can be determined as  $f_p = 1/\sqrt{LC}$ . The single resonator provides a pass band with a high  $Q$ -factor. For the parallel  $LC$  resonator, the  $Q$ -factor is estimated by  $Q = \sqrt{C_1^2/L_1^2}$ .

To obtain an ideal bandpass, the parallel resonator should have a lower inductance and higher capacitance to obtain a high  $Q$ -factor. The equivalent circuit was modelled and simulated using ADS software. The values of the  $LC$  parameters are calculated Liu et al. (2020) and verified through the values of ADS software. It is observed that the simulated result obtained from the ECM is in agreement with that obtained bandpass FSS result, which verifies the validity of the ECM shown in Fig. 5. The approximate equations of the calculated values are as follows:

$$C = C_p \left( 1 - \left( \frac{f_p}{f_z} \right)^2 \right)^2 \quad (1)$$

$$L = \frac{1 - (f_p/f_z)^2}{C(2\pi f_p)^2} \quad (2)$$

In which,

$$C_p = \frac{\varepsilon_r}{2\pi BW_{TP} Z_0} \quad (3)$$

where,  $\varepsilon_r$  is the relative permittivity of the dielectric substrate,  $BW_{TP}$  is the bandwidth of the parallel resonant frequency,  $L$  is the inductance, and  $C$  is the capacitance. Here,  $f_z$  will be zero since there is no rejection band.

### 3. Performance Analysis of the Bandpass FSS

#### 3.1. Parametric Analysis

The primary reason for the wide bandwidth and minimum insertion loss ( $<0.1$  dB) of the proposed bandpass unit cell is the incorporation of the meander line in the etched rhombus slot. Thus, the influence of the length and width of the meander line is studied in this section. The width of the meander line corresponds to the desired bandwidth, and its effect is plotted in Fig. 6 (a). The value of the  $w_l$  is fixed as 0.25 mm based on the quarter wavelength calculation. If the  $w_l$  is decreased from 0.25 to 0.2 mm, the resonant frequency can be tuned to 10 GHz to 11.5 GHz. A value of above 0.28 mm results in a frequency shift of 1.2 %, and make the structure bulkier. Furthermore, by varying  $w_l$  the lower and higher frequency at 1 and 22 GHz remains constant without any change in the roll-off characteristics. The lower frequency is controlled by the length of the meander line denoted by  $l_3$ . This parameter induced a variation in the roll-off characteristics in the higher frequency. The decrease in the  $l_3$  leads to a reduction of the desired X-bandwidth. By increasing  $l_3$ , the lower frequency is tuned and also produces a slight variation in the roll-off characteristics. Throughout the variation in the higher frequency, the roll-off in the higher frequency remains constant. Thus, it is inferred from Fig. 6(b) that the roll-off characteristics in lower and higher frequencies are independent of each other behaviors.

#### 3.2. Angular Stability

The transmission spectrum of the proposed bandpass FSS under different oblique incidences was analyzed. The angular stability for incident angles  $0^\circ$  to  $60^\circ$  for TE and TM mode in steps of  $15^\circ$  is depicted in Fig. 7(a) and Fig. 7(b), respectively. From the figure, it is inferred that the proposed bandpass FSS is stable up to  $60^\circ$ . The resonant frequency is 10 GHz for  $T_p$  and the insertion loss is  $<0.1$  dB at the normal incident angle in both TE and TM modes. For  $T_p$ , the center frequency is shifted only by 1% and also maintains a stable insertion loss till  $0^\circ$  to  $60^\circ$ . However, an unavoidable spurious response is induced at 18 GHz. This is mainly due to the reduced tolerance of the etched slots designed for achieving the required frequencies. Thus, when the angle of incidence increases the parasitic resonance is created Dong et al. (2021). Overall, the proposed FSS is stable, especially when the incident angle is as high as  $60^\circ$ . Owing to the symmetric structure, the frequency response of the proposed bandpass FSS is independent from

the polarization angle. These characteristics offer excellent flexibility for the proposed structure to be exploited in several applications.

A comparison between the proposed FSS with other reported works is illustrated in Table 1. It is inferred that the proposed FSS has the slightest frequency shift and stable angular performance when compared with other states of the art.

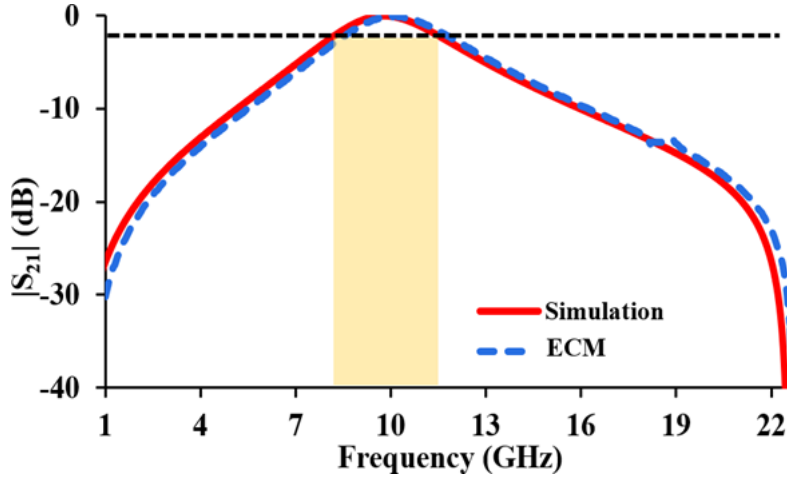


Figure 5. Comparison of ECM and simulation result

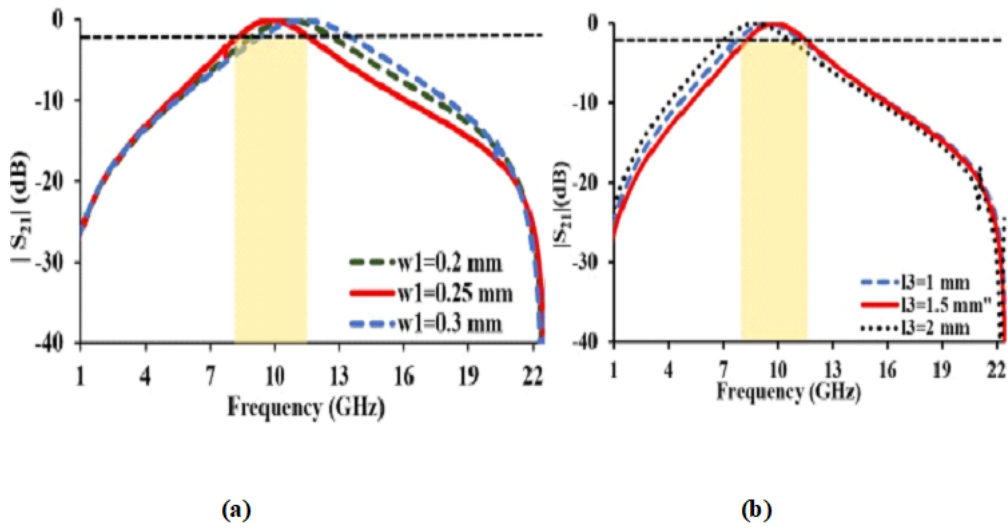
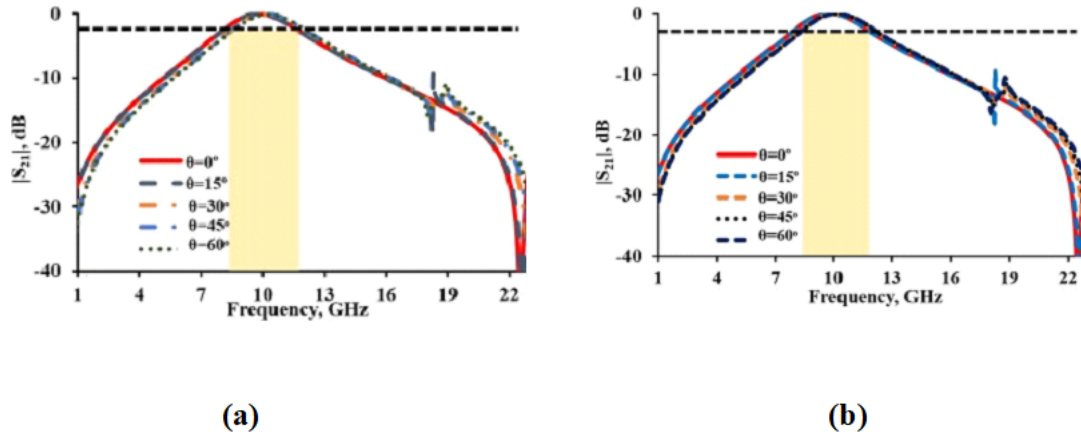


Figure 6. Effect of the meander line width ( $w_1$ ) at  $T_p$  and bandwidth, and (b) Effect of the meander line length  $l_3$  at 1 GHz (roll-off)

#### 4. Fabrication and Measurement

The measurement set-up of the bandpass FSS in front and side view is shown in Fig. 8(a), and Fig. 8(b), respectively. Fig. 8(c) depicts an array of  $48 \times 48$  cells, fabricated on the conformal polyimide substrate with a profile of 0.05 mm. The bending view of the prototype is shown in Fig. 8(d). The proposed bandpass FSS is measured using a Vector Network Analyzer (VNA) with a connected pair of low-frequency horn antennas. Good agreement between the measured and simulated results is shown in Fig. 9(a). The measured result shows a wider performance from 7 to 13 GHz with an insertion loss of 0.13 dB. The Simulated bending performance of the proposed FSS is depicted in Fig. 9(b) to verify the conformal operation. The prototype is fixed on the foam with a curvature of  $120^\circ$ . Using the formula in Zargar et al. (2021),  $r = \frac{80A}{\pi Dc}$  the

radius of the foam is measured. Here,  $A$  is the arc length, and  $DC$  is the degree of the  $180^\circ$ . The prototype is fixed in the foam with a radius of 92.5 mm. The comparison between the simulated and measured results for the bending analysis is shown in Fig. 9(b). It is inferred that by bending the prototype into  $150^\circ$  and  $180^\circ$ , there is a slight variation in the performance in the transmission characteristics which is acceptable. The actual response is achieved till  $180^\circ$  curvature that confirms the enhanced conformality of the proposed FSS. The proposed bandpass FSS exhibits a wider



**Figure 7.** Simulated transmission coefficients  $|S_{21}|$  of the proposed conformal FSS (a) TE mode, (b) TM mode

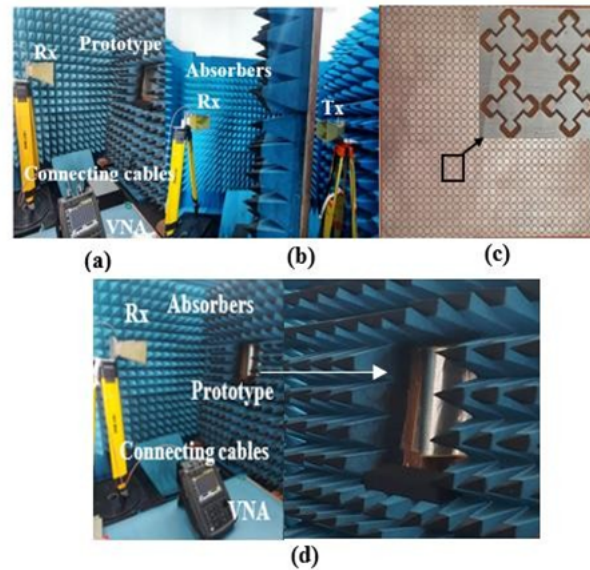


**Figure 8.** Measurement Set-up of the bandpass FSS (a) Front view, (b) Side view, (b) Fabricated Prototype (Inset: Magnified view), (d) Bending analysis

transmission bandwidth of 4.12 GHz (7.98-12.1 GHz), lower insertion loss of 0.1 dB, and stable angular performance up to  $60^\circ$  without using several advances [Li et al. \(2020\)](#), [Al-Joumayly and Behdad \(2010\)](#), [Wang et al. \(2022\)](#), [Liu et al. \(2017\)](#), [Liu et al. \(2020\)](#), [Dong et al. \(2021\)](#), [Zhou et al. \(2022\)](#), [Zhu et al. \(2018\)](#) and [Zhao et al. \(2019\)](#). Thus, the proposed FSS is suitable for X-band RADAR communication applications. Table 2 compares the quantitative of the proposed bandpass FSS with other states of the art.

- The FSS has a reduced geometry of above 67%, 60%, 30%, 4%, and 41% as compared to

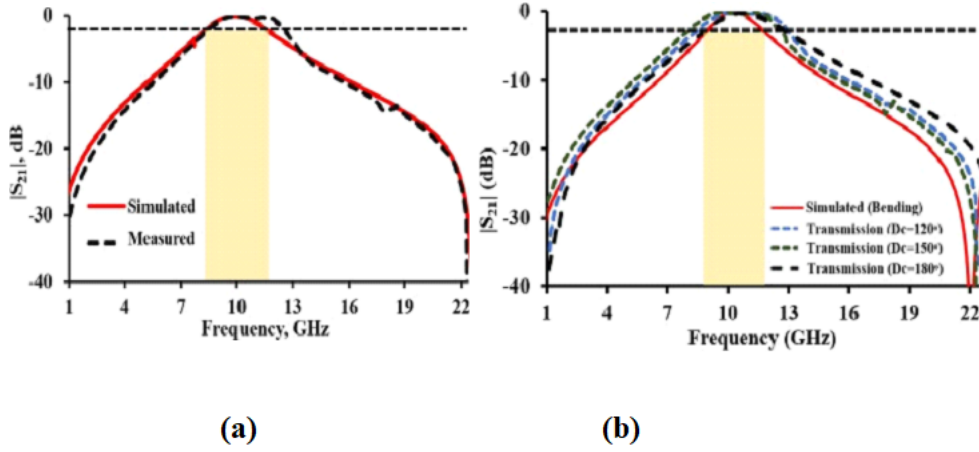


**Figure 9.** (a) Simulated and measured  $S_{21}$  for proposed bandpass FSS, (b) Bending analysis at different angles

**Table 2.** Quantitative Comparison With Other Relevant Bandpass FSS

References	UCS ( $\lambda_0 \times \lambda_0$ )	Profile (mm)	Freq/BW (GHz)	IL (dB)	$\theta$
Li et al. (2020)	0.17	1.53	10-10.5/0.5	0.86	40°
Liu et al. (2017)	0.762	0.76	2.5-6.5/4	1.2	40°
Zhu et al. (2018)	0.63	0.8	6.8-11.5/4.7	0.6	40°
Zhao et al. (2019)	0.29	10	2.9-3.3/0.4	2.1	40°
Zargar et al. (2021)	0.26	1	14-16.2/2.2	1	20°
Jiang et al. (2024)	0.43	0.1	9.2-10.2/1	0.5	-
Afzal et al. (2023)	0.11	10	3.2-3.9/0.7	0.5	60°

Liu et al. (2017), Zhu et al. (2018), Zhao et al. (2019), Zargar et al. (2021) and Jiang et al. (2024).

- The reported works in Li et al. (2020), Liu et al. (2017), Zhao et al. (2019) and Zargar et al. (2021) have obtained lower bandwidth (<4 GHz) even by designing the unit cell in stacked, double-printed, and cascaded forms. In stacked and cascaded structures, the higher profile is used to design the unit cell which is not preferred for several applications Liu et al. (2017). However, the proposed bandpass FSS has achieved 4.12 GHz by developing the simple unit cell on a conformal substrate.
- The proposed unit cell is developed on a flexible substrate with a thickness of 0.05 mm. The works reported in Li et al. (2020), Liu et al. (2017), Zhu et al. (2018), Zhao et al. (2019), Zargar et al. (2021), Jiang et al. (2024) and Afzal et al. (2023) have used higher profiles to achieve the desired features.
- To obtain the lower insertion loss, the works reported in Li et al. (2020), Liu et al. (2017), Zhu et al. (2018), Zhao et al. (2019) and Zargar et al. (2021) have used stacked, cascaded

structures, and double-printed substrates on both sides of the metallic layer. The lower insertion loss of 0.1 dB is utilized in the proposed FSS without exploiting these methods.

- The FSS reported in Li et al. (2020), Liu et al. (2017), Zhu et al. (2018), Zhao et al. (2019) and Zargar et al. (2021) provides lower angular stability ( $<40^\circ$ ) as compared to the proposed FSS ( $60^\circ$ ).

## 5. Conclusions

A conformal bandpass FSS is proposed for RADAR applications. The bandpass FSS operates at a frequency from 7.8 to 12.1 GHz which makes it suitable for X-band Radome applications. The insertion loss of the bandpass FSS is  $<0.1$  dB without using stacked, and cascading structures. It provides a wider bandwidth of 4.12 GHz with a stable angular performance of  $60^\circ$  that makes it a good candidate for the Radome wall. The measured performance is estimated with the simulated results and is suitable for X-band RADAR Communication, and Radome applications.

## References

- Abadi, S. M. A. M. H and Behdad, N. Inductively-coupled miniaturized-element frequency selective surfaces with narrowband, high-order bandpass responses. *IEEE Transactions on Antennas and Propagation*, 63, 2015. ISSN 0018926X. doi: 10.1109/TAP.2015.2477850.
- Afzal, W; Ebrahimi, A; Robel, M. R, and Rowe, W. S. Low-profile higher-order narrowband bandpass miniaturized-element frequency-selective surface. *IEEE Transactions on Antennas and Propagation*, 71, 2023. ISSN 15582221. doi: 10.1109/TAP.2023.3239171.
- Al-Joumayly, M and Behdad, N. A new technique for design of low-profile, second-order, bandpass frequency selective surfaces. *IEEE Transactions on Antennas and Propagation*, 57, 2009. ISSN 0018926X. doi: 10.1109/TAP.2008.2011382.
- Al-Joumayly, M. A and Behdad, N. A generalized method for synthesizing low-profile, band-pass frequency selective surfaces with non-resonant constituting elements. *IEEE Transactions on Antennas and Propagation*, 58, 2010. ISSN 0018926X. doi: 10.1109/TAP.2010.2078474.
- Cahill, R; Vardaxoglou, J. C, and Jayawardene, M. Two-layer mm-wave fss of linear slot elements with low insertion loss. *IEE Proceedings: Microwaves, Antennas and Propagation*, 148, 2001. ISSN 13502417. doi: 10.1049/ip-map:20010767.
- Chen, G. W; Wong, S. W; Li, Y; Chen, R. S; Zhang, L; Rashid, A. K; Xie, N, and Zhu, L. High roll-off frequency selective surface with quasi-elliptic bandpass response. *IEEE Transactions on Antennas and Propagation*, 69, 2021. ISSN 15582221. doi: 10.1109/TAP.2021.3060148.
- Dong, J; Ma, Y; Li, Z, and Mo, J. A miniaturized quad-stopband frequency selective surface with convoluted and interdigitated stripe based on equivalent circuit model analysis. *Micromachines*, 12, 2021. ISSN 2072666X. doi: 10.3390/mi12091027.
- Hussein, M; Zhou, J; Huang, Y, and Al-Juboori, B. A low-profile miniaturized second-order bandpass frequency selective surface. *IEEE Antennas and Wireless Propagation Letters*, 16, 2017. ISSN 15361225. doi: 10.1109/LAWP.2017.2746266.
- Jiang, M; Du, Z; Li, Y; Sun, S, and Hu, J. Frequency-selective surfaces with quasielliptic bandpass response for filtering fra application. *IEEE Transactions on Antennas and Propagation*, 72(1): 1004–1008, 2024. doi: 10.1109/TAP.2023.3311144.
- Li, H; Li, B, and Zhu, L. Wideband bandpass frequency-selective structures on stacked slotline resonators: Proposal and synthetic design. *IEEE Transactions on Antennas and Propagation*, 68, 2020. ISSN 15582221. doi: 10.1109/TAP.2020.2993312.
- Liu, N; Sheng, X; Zhang, C; Fan, J, and Guo, D. A feasible bandwidth compensation technique for fss radome design. *IEICE Electronics Express*, 14, 2017. ISSN 13492543. doi: 10.1587/elex.14.20170510.

- Liu, N; Sheng, X; Zhang, C, and Guo, D. Design and synthesis of band-pass frequency selective surface with wideband rejection and fast roll-off characteristics for radome applications. *IEEE Transactions on Antennas and Propagation*, 68, 2020. ISSN 15582221. doi: 10.1109/TAP.2019.2955665.
- Munk, B. A and Munk, B. A. Munk ba. frequency selective surfaces: theory and design. *Wiley-Interscience: New York*, 2000.
- Sarabandi, K and Behdad, N. A frequency selective surface with miniaturized elements. *IEEE Transactions on Antennas and Propagation*, 55, 2007. ISSN 0018926X. doi: 10.1109/TAP.2007.895567.
- Vegesna, S; Zhu, Y; Bernussi, A, and Saed, M. Terahertz two-layer frequency selective surfaces with improved transmission characteristics. *IEEE Transactions on Terahertz Science and Technology*, 2, 2012. ISSN 2156342X. doi: 10.1109/TTHZ.2012.2202035.
- Wang, D. S; Zhao, P, and Chan, C. H. Design and analysis of a high-selectivity frequency-selective surface at 60 ghz. *IEEE Transactions on Microwave Theory and Techniques*, 64, 2016. ISSN 00189480. doi: 10.1109/TMTT.2016.2557325.
- Wang, P; Jiang, W; Hong, T; Li, Y; Pedersen, G, and Shen, M. A 3-d wide passband frequency selective surface with sharp roll-off sidebands and angular stability. *IEEE Antennas and Wireless Propagation Letters*, 21, 2022. ISSN 15485757. doi: 10.1109/LAWP.2021.3126890.
- Yan, M; Qu, S; Wang, J; Zhang, A; Zheng, L; Pang, Y, and Zhou, H. A miniaturized dual-band fss with second-order response and large band separation. *IEEE Antennas and Wireless Propagation Letters*, 14, 2015. ISSN 15361225. doi: 10.1109/LAWP.2015.2413942.
- Zargar, M. M; Rajput, A; Saurav, K, and Koul, S. K. Single-layered flexible dual transmissive rasorbers with dual/triple absorption bands for conformal applications. *IEEE Access*, 9, 2021. ISSN 21693536. doi: 10.1109/ACCESS.2021.3126197.
- Zhao, Z; Zhang, A; Chen, X; Peng, G; Li, J; Shi, H, and Kishk, A. A. Bandpass fss with zeros adjustable quasi-elliptic response. *IEEE Antennas and Wireless Propagation Letters*, 18, 2019. ISSN 15485757. doi: 10.1109/LAWP.2019.2911908.
- Zhou, H; Hong, W; Tian, L, and Jiang, M. A polarization-rotating siw reflective surface with two sharp band edges. *IEEE Antennas and Wireless Propagation Letters*, 15, 2016. ISSN 15361225. doi: 10.1109/LAWP.2015.2433174.
- Zhou, X; Sun, R; Zhao, P; Cao, Y; Yuan, B; Chen, S, and Wang, G. A novel design of a compact frequency-selective surface with high selectivity and angular stability. *IEEE Microwave and Wireless Components Letters*, 32, 2022. ISSN 15581764. doi: 10.1109/LMWC.2022.3153123.
- Zhu, J; Tang, W; Wang, C; Huang, C, and Shi, Y. Dual-polarized bandpass frequency-selective surface with quasi-elliptic response based on square coaxial waveguide. *IEEE Transactions on Antennas and Propagation*, 66, 2018. ISSN 0018926X. doi: 10.1109/TAP.2018.2794386.